Proceedings of
11th European Conference on Turbomachinery Fluid dynamics & Thermodynamics
ETC11, March 23-27, 2015, Madrid, Spain

REALISTIC VELOCITY AND TURBULENCE INTENSITY PROFILES AT THE COMBUSTOR-TURBINE INTERACTION (CTI) PLANE IN A NOZZLE GUIDE VANE TEST FACILITY

I. Cresci[1], P.T. Ireland[1], M. Bacic[1], I. Tibbott[2], A. Rawlinson[2]

[1]Department of Engineering Science, Parks Road, Oxford, UK, OX1 3PJ
[2]Turbine Systems, Rolls Royce PLC, Derby, UK, DE24 8BJ

ABSTRACT

The continuous demand from the airlines for reduced jet engine fuel consumption results in increasingly challenging high pressure turbine nozzle guide vane (NGV) working conditions. The capability to reproduce realistic boundary conditions in a rig at the combustor-turbine interaction plane is a key feature when testing NGVs in an engine-representative environment. A large scale linear cascade rig to investigate NGV leading edge cooling systems has been designed with particular attention being paid to creating engine representative conditions at the inlet to the NGVs. The combustor simulator replicates the main features of a rich-burn design including large dilution jets and extensive endwall film cooling. CFD simulations have been used to match Reynolds number and mainstream-to-dilution jet momentum flux ratio; velocity and turbulence measurements have been acquired at the NGV inlet plane at ambient temperature. These results show that the velocity and the turbulence intensity distributions are dominated by the endwall cooling flows, and that the measured turbulence length scales reflect the scale of the relevant upstream jets.

NOMENCLATURE

A/D	Analog-to-digital	p	Pitchwise coordinate	u	Velocity
CFD	Computational Fluid Dynamics	PSD	Power Spectrum Density	$\overline{u}$	Mean velocity
				u'	Turbulent fluctuation
CTI	Combustor-Turbine Interaction Rig	r'	Distance	**Greek Alphabet**	
		R_{uu}	Autocorrelation	ε	Turbulent dissipation
CTA	Constant Temperature Anemometer	RANS	Reynolds-Averaged Navier-Stokes	η	Dynamic viscosity
				κ	Turbulent kinetic energy
D	Diameter	Re	Reynolds number	λ	Length scale
D_h	Hydraulic diameter	RIDN	Rear Inner Discharge Nozzle	Λ	Integral length scale
e	Error			ν	Kinematic viscosity
H	Spanwise length	RODN	Rear Outer Discharge Nozzle	ρ	Density
J	Jet-to-mainstream momentum flux ratio			τ	Time lag
		RQL	Rich-Burn, Quick - Mix, Lean-Burn combustor	T	Integral time scale
k	Wavenumber			**Subscripts**	
L	Pitchwise length			c	Coolant conditions
LES	Large Eddy Simulation	s	Spanwise coordinate	i	i-th sample
$\dot{m}$	Mass flow	t	Time	rms	Root mean square
NGV	Nozzle Guide Vane	Tu	Turbulent intensity	∞	Mainstream conditions

INTRODUCTION

The flow at the combustor-turbine interaction plane is complex and, up to now, has frequently been idealized as a uniform field in both experimental set-ups and CFD simulations. This simplification has been shown to limit the accuracy of the experimental simulation of flow through a turbine

cascade (Ames [1997] , Qureshi et al. [2011]).

The principal goal of the work presented in this paper is to reproduce the main flow features present downstream of a Rich-Burn, Quick-Mix, Lean-Burn (RQL) combustor in a low speed linear cascade. The wind tunnel has been designed for a high resolution investigation of leading edge film cooling in high pressure NGVs to generate highly detailed data that can be used for the validation of CFD simulations.

RQL combustors are preferred at present because of reduced cost, weight, fuel burn, noise and improved combustion stability. In RQL combustors a primary rich-burn zone at high temperature allows to minimize the production of incomplete combustion products (i.e. soot and carbon monoxide). Dilution air from the compressor is introduced downstream of the primary combustion zone to quench the combustion process and to reduce the peak flow temperature to acceptable levels for the NGVs and control the NOx formation (Lefebvre [1999] and Samuelsen [2006]). More air is introduced further downstream through the Rear Inner Discharge Nozzle (RIDN) and the Rear Outer Discharge Nozzle (RODN) to control the endwall temperature.

Literature Review

The importance of achieving realistic boundary conditions at the Combustor Turbine Interaction (CTI) plane is reported in several studies. Ames [1997] asserted that turbulence has a significant effect on NGV stagnation region and pressure surface heat transfer. Moss [1992] stated that combustion has negligible effects on turbulence levels and dilution jets govern the mainflow features. In particular the jet-to-mainstream momentum flux ratio dictates the combustor exit velocity, turbulence and temperature profiles (Thole et al. [1994], Vakil and Thole [2005], Barringer et al. [2002], Barringer et al. [2004]). Holdeman [1993] reviewed computational and experimental studies of single, double and opposed rows of dilution jets in a non-reacting combustor. According to his results the k-ε turbulence model is not able to accurately predict the mixing of opposed jets but it succeeds in predicting the jet penetration. Experimental studies have been conducted at Virginia Polytechnic Institute: Thole et al. [1994] compared a turbulence generator, where turbulence levels are adjusted by changing the jet-to-mainstream velocity ratio or the Reynolds number, to a bar-grid turbulence generator. They concluded that the turbulence decay rate is strongly affected by the jet-to-mainstream velocity ratio. Barringer et al. [2002] designed a combustor simulator to evaluate the development of thermal and velocity fields downstream of a realistic combustor, with a particular focus on the effect of dilution jets. Total pressure, mean and turbulent velocity and temperature measurements are reported. Further measurements are shown by Vakil and Thole [2005]. Barringer et al. [2002] and Vakil and Thole [2005] results prove once more the dominance of the dilution jets and show a large recirculation region downstream of the jet injection. The apparatus studied by Colban et al. [2003] and Barringer et al. [2002] was modelled and simulated by Stitzel and Thole [2004]: RANS simulations with RNG k-ε turbulence model with non-equilibrium wall functions underpredicted turbulence compared to the measurements. Previous studies on combustor simulators at the University of Oxford are reported by Povey and Qureshi [2009] and Qureshi et al. [2011]: significant heat transfer variations on vanes and endwalls between an uniform temperature boundary condition and a distorted temperature profile case were found, mainly due to changes in the local gas driving temperature. Thomas et al. [2013] designed a combustor simulator for a low-speed linear cascade facility, able to match Reynolds number and jet-to-mainstream momentum flux ratio to engine conditions, but no traverse measurements were taken downstream the apparatus. Cha et al. [2012a], [2012b] took detailed flow measurements downstream a fully featured rich-burn engine combustor at Loughborough University and compared them to RANS and LES simulations. Because RANS models tend to be overly dissipative, the k-ε tends to overpredict the turbulence levels at the interface plane, but the distributions show a good agreement with the experimental data.

The goal of the present work is to design a flexible combustor simulator to be installed upstream of a large scale NGV cascade and to use it to obtain high resolution velocity and turbulence measurements and to compare them to RANS calculations run at the same rig conditions. The data will be used to produce engine representative conditions at the inlet of a large-scale cascade.

EXPERIMENTAL SET-UP

The tests were carried out in a continuous large-scale low-speed linear cascade facility in the Osney Laboratory (University of Oxford). The wind tunnel is capable of 100 m/s at the vane throat (3.2 kg/s through the test section) and is fitted with a 150 kW heater mesh (Ireland and Jones [2000]) ahead of the test section. The vane chord is 263 mm.

The heater mesh was not used for the tests presented in this paper: the results are all calculated and measured in isothermal conditions.

Combustor-Turbine Interaction Rig

The CTI rig is shown in Figure 1. A primary air flow replicates the main hot gas flow and a secondary air stream represents the coolant path. The mainstream air enters the inlet contraction which is designed to produce a uniform exit velocity profile. A heater mesh (400x500 mm^2, 38% open area) provides a step rise to the inlet temperature up to 50 K. The coolant flow is injected into the mainflow through a combustor simulator. At its exit, a 267x500 mm^2 straight duct, fitted with a traverse mechanism, allows the velocity to be measured. A diffuser connects the test section to the suction fan. The coolant flow is provided by a secondary fan and passes through four different pipes that feed four separate plenums: one feeds the outer dilution ports, one the inner dilution ports, one the RIDN rows and one the RODN rows. This allows considerable flexibility in the test set-up.

Figure 1: **CTI Rig: Tunnel inlet (left) and close up of test section (right)**

Combustor Simulator

The combustor simulator CAD model and its major features are shown on the left hand side of Figure 2. In the CTI rig, dilution ports, RIDN and RODN are engine representative (Thomas et al. [2013]); the main geometrical parameters are reported in Table 1. In the centre of Figure 2 the location of measurement planes is presented: plane A is downstream of the dilution flow injection and upstream of the cross-section reduction; plane B is inside the contraction; plane C is downstream of it; plane D is between the first and the second nozzle row and plane E coincides with the NGV inlet plane. Plane E is the only location where experimental data are available.

Measurement Instrumentation

The mass flow through the coolant pipes is measured using four orifice meters according to ISO 5167-22003. A two-axis computer-controlled traverse system moves a probe across the NGV inlet plane. The traverse system comprises two Mclennan 23HSX202CI500L stepper motors connected

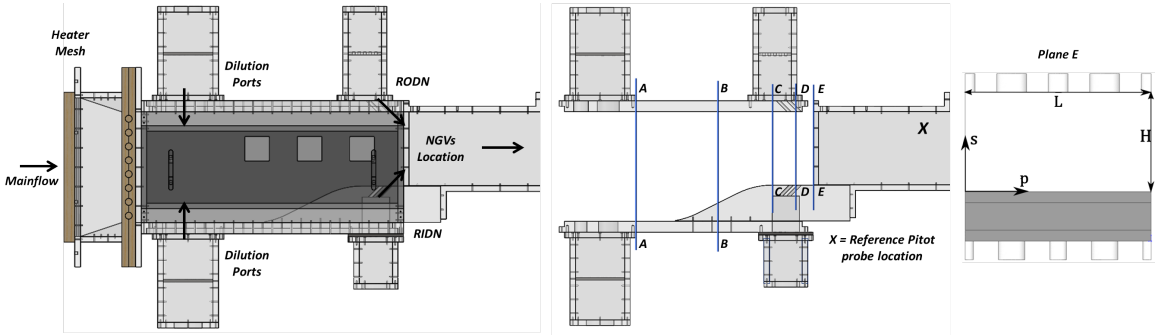

Figure 2: **Combustor Simulator: Flowpaths (left), measurement plane locations (centre), coordinate system at plane E (right)**

	Hole diameter [mm]	Inclination [deg]	Pitch [mm]
Inner wall big dilution ports	71	90	250
Inner wall small dilution ports	44.5	90	250
Outer wall big dilution ports	80	90	250
Outer wall small dilution ports	53.5	90	250
RIDN	9	45	22
RODN	9	45	18

Table 1: **Geometrical dimensions**

to two ST5-Q-NN stepper drivers and controlled with a NI-PCI6220 card. The velocity map was measured with a four-hole pressure probe (Main et al. [1996] ,Tsang [2002], Goodman [2007]). It was calibrated by Forsyth et al. [2014] as described by Telisinghe and Gillespie [2006], using a strategy similar to Main et al. [1996] adapted for low Mach number flows. Turbulence information was acquired using a Dantec Dynamics 55P11 miniature $5\mu m$ single wire sensor and a Dantec Dynamics StreamLine Pro CTA system. The hot-wire was calibrated before and after each test fitting the voltage output to that measured by a Pitot probe installed in the wind tunnel to King's power law $E^2 = A + BU_{wire}^{0.45}$ (Dantec [2002]).

Uncertainty analysis

Moffat [1988] states that if the result R of an experiment is a function of N independent variables X, the individual uncertainty terms can be combined by a root-sum-square method $\partial R = \sqrt{\sum_{i=1}^{N} \left(\frac{\partial R}{\partial X_i}\partial X_i\right)^2}$. Following this procedure and considering uncertainties in temperature and pressure measurements and in the calibration process, the most likely overall uncertainty on the four-hole probe velocity calculations is 6%. In order to calculate the uncertainty on the coolant massflow calculated with orifice meters, the input values of pressure and density were perturbed as suggested by Moffat for results that are difficult to differentiate: the resulting uncertainty is about 6%. The uncertainty on the hot-wire wire results was calculated following the guide by Yavuzkurt [1984]: according to him, the mean value and rms fluctuations of velocity have the same uncertainty and for the measurements presented in this paper it is around 5%. This value agrees with that one calculated using the procedure described in Dantec's manual [2002].

CFD SIMULATIONS

CFD simulations of the combustor simulator at the rig conditions were performed to support understanding of the flow at the combustor turbine interaction plane.

Computational domain and boundary conditions

The computational mesh was generated with ANSYS ICEM 12.0 and contains $1.2 \cdot 10^7$ elements (Fig.3). RANS simulations were performed using Fluent 12.0: the turbulence was simulated using a realizable k-ε turbulence model with enhanced wall treatment, consistent with the approach used by Cha et al. [2012a]. All the inlet total pressure boundaries were set at rig conditions and turbulence levels at 20%, as used by Cha et al. [2012a] in their RANS simulations. It is important to note that inlet turbulence had little effect on turbulence intensity at the exit plane: simulations showed that a variation of 5% of inlet turbulence intensity causes a maximum variation of 0.1% on the turbulence intensity at plane E, confirming that the turbulence levels at the NGV inlet plane are dictated by the dilution jets configuration (Fig.4). The coolant inlet conditions were applied at the plenum inlets, so the computational mesh extended into the plenums. An uniform static pressure boundary condition was applied at the outlet section. Wall boundaries were set on the side walls to match the computational domain with the experimental facility.

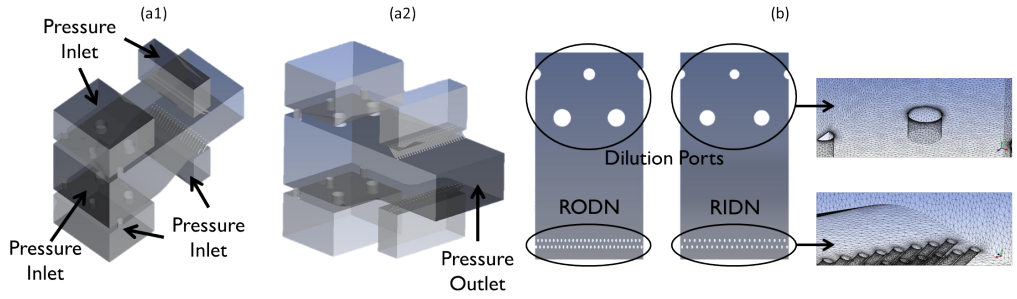

Figure 3: **Computational model and mesh: (a1) Inlet boundary planes; (a2) Outlet boundary plane; (c) Dilution ports and film holes configuration on the endwalls with mesh details**

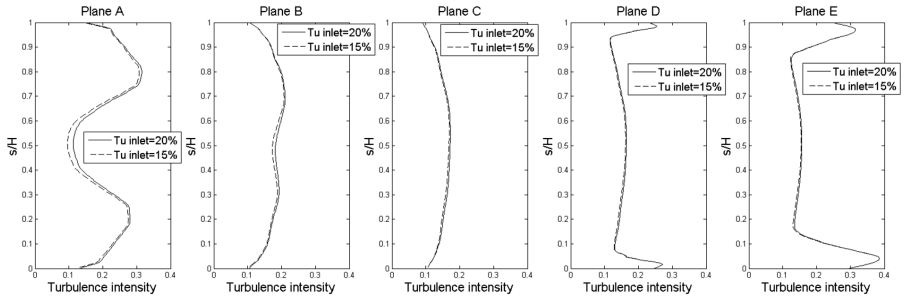

Figure 4: **CFD predictions of turbulence intensity profile averaged in the radial direction: inlet turbulence intensity effect**

RESULTS AND DISCUSSION

In this section the CFD prediction and the acquired velocity measurements are presented and discussed. All data presented in this paper were simulated and acquired at ambient temperature.

Velocity Field

The velocity field was calculated over the entire computational domain and experimental data were acquired at the NGV inlet plane coincident with plane E (Fig. 2). In this section the results obtained at typical engine flow conditions (see Table 2) are presented.

The jet-to-mainstream momentum flux ratio is defined as $J = \frac{\rho_c \cdot v_c^2}{\rho_\infty \cdot v_\infty^2}$.

Reynolds number Re		$^1Re_\infty = 6 * 10^5$
Jet-to-mainstream momentum flux ratio J	Dilution ports	$J = 9$
	RIDN	$J = 11$
	RODN	$J = 6$

Table 2: **Flow conditions**

[1] based on the averaged velocity at the combustor outlet plane and the relative hydraulic diameter

In Figure 5 the flow velocity distribution predicted by the CFD simulation at two different streamwise planes (p/L=0.5 and p/L=1) is normalized by the maximum jet velocity. J is the same for all the dilution jets. A noticeable low-velocity region is visible downstream of each jet injection, as it was previously reported by Vakil and Thole [2005]. An earlier acceleration of flow near the inner inclined flow is also evident. The jet streamlines in Figure 5 show the jet development in the computational domain. The dilution jet dissipation increases close to the bottom wall due to the acceleration caused by the slope.

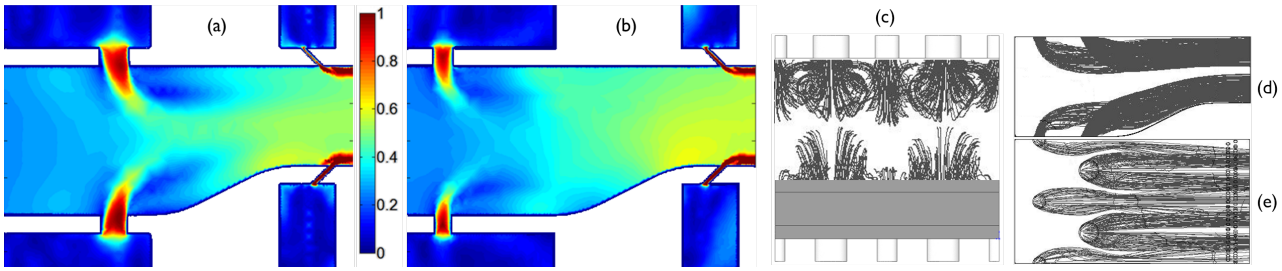

Figure 5: **CFD predictions of (a) normalized velocity v/v_{max} at p/L=1 (view from the side wall), (b) normalized velocity v/v_{max} at p/L=0.5 (view from the side wall), (c) jet streamlines (view from the exit plane), (d) jet streamlines (view from the side wall), (e) jet streamlines (view from the outer wall)**

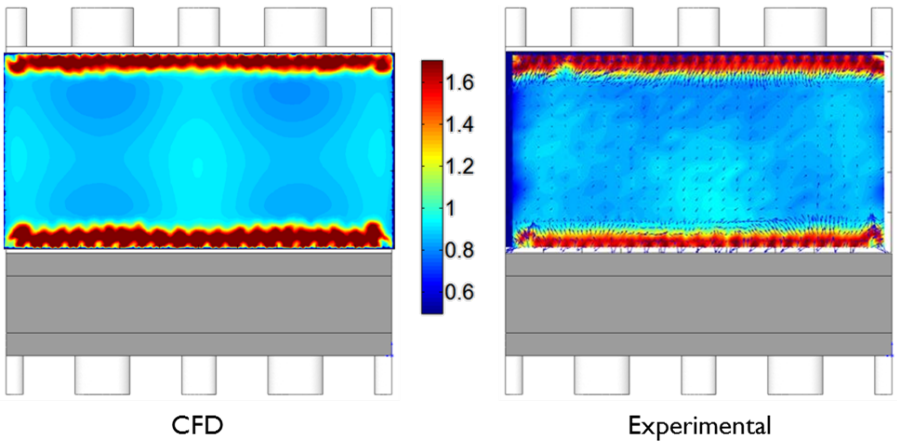

Figure 6: **CFD predictions (left) and experimental measurements (right) of normalized velocity** v/v_{av}

Figure 6 shows the flow velocity non-dimensionalized with the plane area-averaged velocity on the NGV inlet plane (plane E in figure 2) predicted by CFD and measured experimentally in the CTI rig. The flow is mostly uniform away from walls with velocity variations within 3% due to the

blockage caused by the big dilution jets from the top wall (Fig. 5). The high velocity flow close to the inner and outer walls has been injected through the RIDN and RODN. The sidewall effect is very small. The level of agreement between CFD and measurements in Figure 6 is very high, even if the realizable k-ε model seems to underestimate the jet diffusion near the walls.

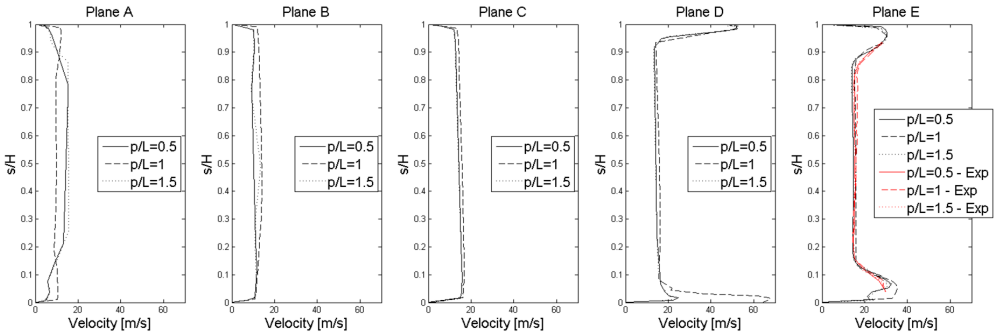

Figure 7: **CFD predictions and experimental measurements of velocity profiles at p/L=0.5 - 1 - 1.5**

Figure 7 shows the velocity boundary layer development along the combustor simulator. The velocity peaks due to the dilution jets at plane A fade away with the flow acceleration (plane B). In plane C the flow near the bottom wall is faster because of the asymmetric contraction. The cooling injection results in a momentum surplus near the endwalls (planes D and E). The mainstream velocity is almost constant from plane C to plane E as there is no change in cross-sectional area. The differences along the radial direction are relevant at plane A but decrease moving downstream: the differences between the velocity profile at off-centerline planes (p/L=0.5 and p/L=1.5) and the centerline plane (p/L=1) are below 2% in the bulk flow for both numerical and experimental data. The agreement between CFD and experiments is very good, with discrepancies below the 1%.

Time spectral analysis

The CTA sampling rate was chosen according to the Nyquist criterion to be higher than twice the system cut-off frequency that was set at 10kHz (so that wavelengths of the order of the millimeter could be resolved). The number of samples was 1 million per data point. The measurement locations are shown in Figure 8.

The autocorrelation between the value of velocity at a fixed point at two different instants t and $(t+\tau)$ is defined as $R_{uu}(\tau) = \frac{\overline{u_i'(t)u_i'(t+\tau)}}{u_i'^2}$. In Figure 9 R_{uu} at points A, B and C is plotted. Because the trends are very similar, R_{uu} at the other locations is not shown. As expected, the coherence of the flow structures lasts longer in the mainflow (point C) than close to the wall and downstream of the coolant injection (points A and B).

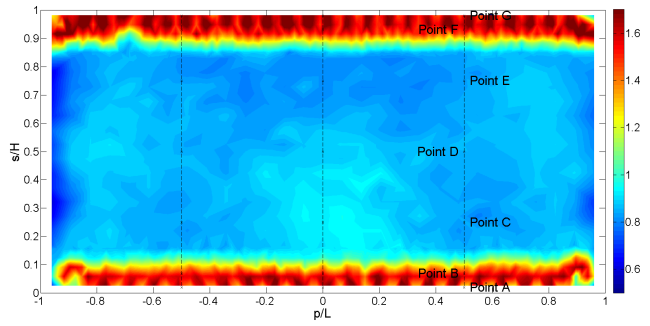

Point	s/H	p/L
A	0.02	0.5 - 1 -1.5
B	0.07	0.5 - 1 -1.5
C	0.25	0.5 - 1 -1.5
D	0.5	0.5 - 1 -1.5
E	0.75	0.5 - 1 -1.5
F	0.93	0.5 - 1 -1.5
G	0.98	0.5 - 1 -1.5

Figure 8: **Hot-wire measurement locations**

From R_{uu} it is possible to calculate the integral time and length scales of the turbulent flow. The integral time scale $T = \int_0^\infty R(\tau)\, d\tau$ is a measure of the average time scale associated with the energy containing eddies in the flow. Assuming Taylor's hypothesis $\frac{\partial}{\partial t} = -\overline{U}\frac{\partial}{\partial x_i}$ (valid for $u'/\overline{u} << 1$ and $Tu < 30\%$, Hinze [1975]), the integral length scale at a fixed point can be calculated as $\Lambda = \overline{u}T$. The Λ distribution (Fig. 9) is symmetrical in the spanwise direction and shows large coherent structures in the bulk flow and smaller structures near the endwalls. The larger eddies are generated by the dilution jets, while the small-scale ones are created by the RIDN and RODN. The length scale values vary in the spanwise direction but the trend is constant. The integral length scales are approximated using an equation suggested by Sykes et al. [1986] ($\Lambda = 0.25D + 0.025r'$, where r' is the distance measured from the dilution port with diameter D). This equation was used to predict the levels in Fig. 9 in the bulk flow: the range boundaries correspond to the smallest and the biggest dilution port diameter (Table 1).

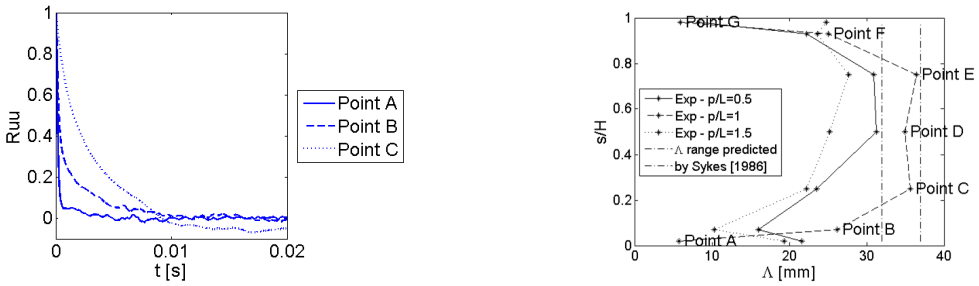

Figure 9: **Autocorrelation function R_{uu} (left) and integral length scale Λ (right)**

The power spectrum density shows how the eddy kinetic energy is distributed among eddies of different wavenumbers, and hence sizes: $PSD(k)dk$ is the energy contained by eddies with wavenumbers between k and $(k + dk)$ and it was evaluated using Welch's method (Mathworks [2004]). The ensemble-averaging of 50 blocks of 1 million samples are used to assure a statistically independent data set. As previously mentioned for R_{uu}, the PSD is plotted only for points A, B and C to avoid data redundancy (Fig. 10). The flow close to the walls (points A and B) is strongly energized by the film injection and has significant kinetic energy at high wavenumber k (corresponding to small wavelength) compared to the mainstream flow.

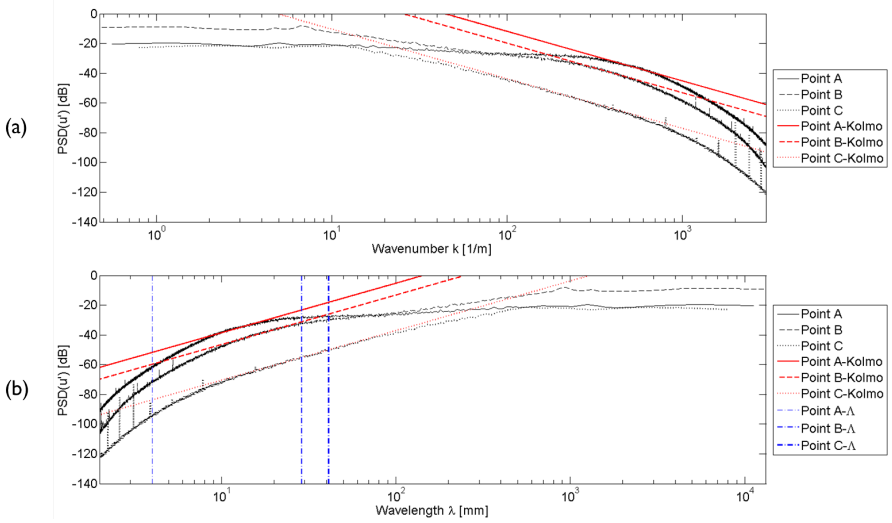

Figure 10: **Power density spectrum: (a) PSD(k) with Kolmogorov's -5/3 power law slope on the left, (b) PSD(λ) with Kolmogorov's -5/3 slope and Λ on the right**

Kolmogorov's theory (Hinze [1975]) states the existence, in turbulent flows with sufficiently high Reynolds number, of a region of the spectrum where the statistics of the small scale motions have a universal form, uniquely determined by the turbulent dissipation rate ε and the kinematic viscosity ν. Within this region the theory identifies the existence of an inertial subrange where the effect of ν is negligible and the spectrum follows the -5/3 power law. This relation holds only if there is no direct effect of the energy-containing eddies, i.e. only if no parameter other than ε and ν affects the turbulence in this region and the spectrum is thereby independent of its conditions of formation. The PSDs calculated by the authors are compared to the Kolmogorov's power law (Fig. 10a): a good correspondence is evident over a wide wavenumber range inside the bulk flow where the PSD plots are tangential to the straight lines with slope -5/3. The inertial subrange is narrower downstream of the film jets: this is because the measurement plane is close to the injection point and turbulence has not settle down. At higher k the slope of the curve changes and the energy contained in the eddies quickly dissipates at a rate depending on both ε and ν. Figure 10b shows the PSD plotted versus the eddy wavelength, $\lambda = \frac{2\pi}{k}$; on the same plot Λ_A, Λ_B and Λ_C are reported. According to Kolmogorov's theory these values should be an estimate of the length scale of the larger eddies: indeed at both points C and B, Λ coincides with the upper limit of the inertial subrange. On the other hand, Λ_A is well below the intersection between the spectrum and the -5/3 power law curve: that is again due to the proximity to the injection point.

The root mean square of the turbulent fluctuation u'_{rms} is obtained by taking the square root of the integral of the PSD with respect to k. The turbulence intensity, $Tu = \frac{u'_{rms}}{u_{mean}}$, profile development along the measurement planes is shown in Figure 11. At plane A the dilution jets strongly affect the profile, but their influence decreases moving in the streamwise direction as the flow accelerates (plane B), becoming progressively more uniform at plane C. Also the radial uniformity increases moving downstream: the maximum difference at plane E between the profiles at the planes at p/L=0.5 - 1 -1.5 is around 3% in the bulk flow for both CFD and experimental data. The endwall cooling injection causes an increase in turbulence levels near the walls: this enhancement is overestimated by the realizable k-ε model compared to the experimental data. Good agreement is reached in the bulk flow with differences within 3%, but with larger differences at the wall. A k-ε model overprediction was also noticed by Cha et al. [2012b]: RANS turbulence modeling tends to be overly predictive and this could justify the differences with the experimental data.

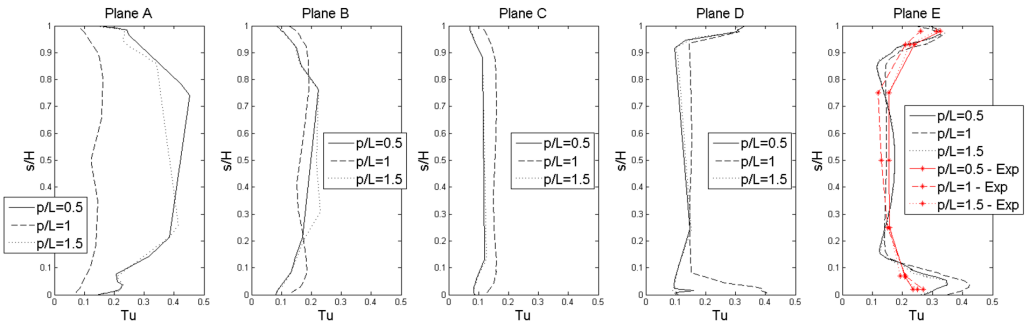

Figure 11: **CFD predictions and experimental measurements of turbulence intensity profiles at p/L=0.5 - 1 - 1.5**

CONCLUSIONS

A highly detailed numerical and experimental investigation of the flowfield at the outlet of a combustor simulator designed for use with a large-scale linear cascade rig at isothermal conditions is presented in this paper. The momentum flux ratio for the dilution and wall film cooling jets was

matched to engine working conditions. The experimental measurements give a complete overview of the velocity field and the turbulent structures and indicate the importance of an engine-representative flow characterization at the combustor-turbine interaction plane. The high resolution data help understand the complex flow field downstream of large dilution jets and endwall film coolant ejection and offer highly detailed CFD validation data.
The research has confirmed the strong influence of the near-wall jets on the velocity and turbulence profiles. A lower, but still significant, effect of the dilution jets on the mainflow is shown, in accordance with prior research work reported in literature. The integral length scales show a connection between the turbulence and the jet injection that has generated it. The PSD plots exhibit good agreement with Kolmogorov's theory: the inertial subrange is evident and its related wavenumber range changes according to the dimensions of the features generating the eddies.

ACKNOWLEDGEMENTS

The research was supported by Rolls-Royce and the UK Ministry of Defence under the ENTAPS project.

The authors are grateful to Prof. P. Denman for guidance on interpreting combustor engine data, to Prof. D. Gillespie for the four-hole probe installation, to Prof. M. McGilvray for the CTA hardware and the Osney Laboratory workshop for manufacturing and assembling the CTI rig.

References

F.E. Ames. The influence of large-scale high-intensity turbulence on vane heat transfer. *Journal of Turbomachinery*, 119(1):23–30, 1997.

M.D. Barringer, O.T. Richard, J.P. Walter, S.M. Stitzel, and K.A. Thole. Flow field simulations of a gas turbine combustor. *Journal of Turbomachinery*, 124(3):508–516, 2002.

M.D. Barringer, K.A. Thole, and M.D. Polanka. Developing a combustor simulator for investigating high pressure turbine aerodynamics and heat transfer. In *ASME Turbo Expo 2004: Power for Land, Sea, and Air*, pages 565–575. American Society of Mechanical Engineers, 2004.

C.M. Cha, S. Hong, P.T. Ireland, P. Denman, and V. Savarianandam. Experimental and numerical investigation of combustor-turbine interaction using an isothermal, nonreacting tracer. *Journal of Engineering for Gas Turbines and Power*, 134(8), 2012a.

C.M. Cha, P.T. Ireland, P.A. Denman, and V. Savarianandam. Turbulence levels are high at the combustor-turbine interface. In *ASME Turbo Expo 2012: Turbine Technical Conference and Exposition*, pages 1371–1390. American Society of Mechanical Engineers, 2012b.

W.F. Colban, G. Zess, A.T. Lethander, and K.A. Thole. Combustor turbine interface studies-part 2: Flow and thermal field measurements. *Journal of Turbomachinery*, 125(2):203–209, 2003.

P. Forsyth, M. McGilvray, and D.D.R.H. Gillespie. Secondary flows and heat transfer coefficient distributions in the developing flow region of ribbed turbine blade cooling passages. In *ASME Turbo Expo 2014*, number GT2014-26737. American Society of Mechanical Engineers, 2014.

J.S. Goodman. *Thermal analysis of ramjet engines*. PhD thesis, University of Oxford, 2007.

J.O. Hinze. *Turbulence*. McGraw Hill, 1975.

J.D. Holdeman. Mixing of multiple jets with a confined subsonic crossflow. *Progress in Energy and Combustion Science*, 19(1):31–70, 1993.

P.T. Ireland and T.V. Jones. Liquid crystal measurements of heat transfer and surface shear stress. *Measurement Science and Technology*, 11(7):969, 2000.

F.E. Jørgensen. How to measure turbulence with hot-wire anemometers - a practical guide, 2002.

A.H. Lefebvre. *Gas Turbine Combustion*. Taylor & Francis, Philadelphia, ii edition, 1999.

A.J. Main, C.R.B. Day, G.D. Lock, and M.L.G. Oldfield. Calibration of a four-hole pyramid probe

and area traverse measurements in a short-duration transonic turbine cascade tunnel. *Experiments in Fluids*, 21(4):302–311, 1996.

Mathworks. pwelch. http://www.mathworks.co.uk/help/signal/ref/pwelch.html, 2004.

R. J. Moffat. Describing the uncertainties in experimental results. *Experimental thermal and fluid science*, 1(1):3–17, 1988.

R.W. Moss. *The Effects of Turbulence Length Scale on Heat Transfer*. PhD thesis, University of Oxford, 1992.

Thomas Povey and Imran Qureshi. Developments in hot-streak simulators for turbine testing. *Journal of Turbomachinery*, 131(3):031009, 2009.

Imran Qureshi, Arrigo Beretta, and Thomas Povey. Effect of simulated combustor temperature nonuniformity on HP vane and end wall heat transfer: an experimental and computational investigation. *Journal of Engineering for Gas Turbines and Power*, 133(3):031901, 2011.

S. Samuelsen. Rich burn, quick-mix, lean burn (RQL) combustor. *The Gas Turbine Handbook, National Energy Technology Laboratory, Editor*, 2006.

S. Stitzel and K.A. Thole. Flow field computations of combustor-turbine interactions relevant to a gas turbine engine. *Journal of Turbomachinery*, 126(1):122–129, 2004.

R.I. Sykes, W.S. Lewellen, and S.F. Parker. On the vorticity dynamics of a turbulent jet in a crossflow. *Journal of Fluid Mechanics*, 168:393–413, 1986.

J.C. Telisinghe and D.D.R.H. Gillespie. Oxford four-hole pressure probe Mk 2 (Probe No.14). Technical report, University of Oxford, Department of Engineering Science, 2006.

K.A. Thole, D.G. Bogard, and J.L. Whan-Tong. Generating high freestream turbulence levels. *Experiments in Fluids*, 17(6):375–380, 1994.

M. Thomas, B. Kirollos, D. Jackson, and T. Povey. Experimental and CFD studies of NGV endwall cooling. In *ASME Turbo Expo 2013: Turbine Technical Conference and Exposition*, pages V03BT13A056–V03BT13A056. American Society of Mechanical Engineers, 2013.

C. Tsang. *High blockage turbulators*. PhD thesis, University of Oxford, 2002.

S.S. Vakil and K.A. Thole. Flow and thermal field measurements in a combustor simulator relevant to a gas turbine aeroengine. *Journal of Engineering for Gas Turbines and Power*, 127(2):257–267, 2005.

S Yavuzkurt. A guide to uncertainty analysis of hot-wire data. *Journal of fluids engineering*, 106(2): 181–186, 1984.